HHS Public Access

Author manuscript

Nat Commun. Author manuscript; available in PMC 2015 January 16.

Published in final edited form as:

Nat Commun. ; 5: 4425. doi:10.1038/ncomms5425.

Src-dependent impairment of autophagy by oxidative stress in a mouse model of Duchenne muscular dystrophy

Rituraj Pal[1], **Michela Palmieri**[2], **James A. Loehr**[1], **Shumin Li**[1], **Reem Abo-Zahrah**[1], **Tanner O. Monroe**[1], **Poulami Basu Thakur**[1], **Marco Sardiello**[2], and **George G. Rodney**[1,*]

[1]Department of Molecular Physiology and Biophysics, Baylor College of Medicine, Houston, TX U.S.A

[2]Department of Molecular Human Genetics, Baylor College of Medicine, Houston, TX U.S.A

Abstract

Duchenne muscular dystrophy (DMD) is a fatal degenerative muscle disease resulting from mutations in the dystrophin gene. Increased oxidative stress and altered Ca^{2+} homeostasis are hallmarks of dystrophic muscle. While impaired autophagy has recently been implicated in the disease process, the mechanisms underlying the impairment have not been elucidated. Here we show that nicotinamide adenine dinucleotide phosphatase (Nox2)-induced oxidative stress impairs both autophagy and lysosome formation in *mdx* mice. Persistent activation of Src kinase leads to activation of the autophagy repressor mammalian target of rapamycin (mTOR) via PI3K/Akt phosphorylation. Inhibition of Nox2 or Src kinase reduces oxidative stress and partially rescues the defective autophagy and lysosome biogenesis. Genetic down regulation of Nox2 activity in the *mdx* mouse decreases ROS production, abrogates defective autophagy and rescues histological abnormalities and contractile impairment. Our data highlight mechanisms underlying the pathogenesis of DMD and identify NADPH oxidase and Src kinase as potential therapeutic targets.

Duchenne muscular dystrophy (DMD) is the most common X-linked lethal disorder in humans. It is caused by mutations in the dystrophin gene [1, 2], resulting in progressive skeletal muscle degeneration and ultimately leading to paralysis and death [3]. While there is intense research focused on gene and cell based therapy, to date there is no cure for DMD. Pharmacological based treatments are aimed at controlling the progression of symptoms, buying time until a genetic or cell based treatment is realized. How dysfunctional pathways in the dystrophic muscle lead to degeneration is still a matter of intense investigation. The characterization of the culprit pathway(s) linking mutations in dystrophin to muscle

*All correspondence should be sent to rodney@bcm.edu..

Author contributions R.P. and G.G.R. conceived and designed the experiments. R.P., M.P., J.A.L., S.L., R.A., and T.O.M. performed the experiments. P.B.T. and G.G.R. designed and created the $p47^{-/-}$-*mdx* mouse model. M.P. and M.S. designed the lysosome experiments. R.P. and G.G.R. wrote the manuscript. All authors have read, edited, and approved the final manuscript.

Competing financial interests The authors declare no competing financial interests.

degeneration will indeed prove critical in the development of new therapeutic approaches in DMD.

Increased Nox2 activity [4, 5] and Src kinase expression [6, 7] are thought to underlie the increased oxidative stress in muscles of the *mdx* mouse, a model of DMD [8]. Recently, impaired autophagy and accumulation of dysfunctional organelles have been reported in dystrophic muscle [9-11], which may underlie muscle degeneration. Because Src kinase can activate Akt via PI3K (Type I) [12-14] leading to a decrease in mammalian target of rapamycin (mTOR)-dependent autophagy [15, 16], we surmised that Nox2 and Src are the critical proteins that link oxidative stress to impaired autophagy in *mdx* skeletal muscle. We found that in dystrophic muscle increased Nox2 activity increases oxidative stress, activates Src kinase, and impairs autophagy by regulating the PI3K/Akt/mTOR pathway.

Results

Nox2 increases oxidative stress in *mdx* mice

Using either the non-specific redox probe DCF (Supplementary Figure 1a) or our Nox2-specific ROS biosensor p47-roGFP [17] (Fig. 1a) we found increased Nox2-specific ROS production in *mdx* skeletal muscle compared to wild-type (WT). The increase in ROS was abolished upon inhibition of Nox2 with the Nox2-specific peptide inhibitor gp91 ds (Fig. 1a, Supplementary Figure 1a&b), scavenging either extracellular or intracellular H_2O_2 (Fig. 1a), or incubating with the antioxidant N-acetyl cysteine (NAC, Supplementary Figure 1c). Additionally, increased Nox2 activity resulted in intracellular oxidative stress as evidenced by oxidation of the glutathione redox potential probe Grx1-roGFP2 (Fig. 1b). *Mdx* skeletal muscle showed an increase in both total and active Rac1 (Fig. 1c & Supplementary Figure 1d), a regulator of Nox2 activity, as well as phosphorylated and total Src kinase (Fig. 1d & Supplementary Figure 1e) protein levels. While the conversion of total Src into active Src (Y416) was significantly higher in *mdx*, no significant difference in conversion of total Rac1 to active Rac1 was observed. We also found that the active phosphorylated form of $p47^{phox}$ was significantly higher in *mdx*, which was blunted upon incubation with gp91 ds or the selective Src inhibitor, PP2 (Fig. 1e). No significant difference in total $p47^{phox}$ expression level was observed. Inhibition of Src and/or Rac1 decreased oxidation of both p47-roGFP (Fig. 1f) and the extracellular H_2O_2 sensor Amplex Red (Fig. 1g) in *mdx* skeletal muscle. Thus, Src and Rac1 play major roles in enhanced ROS generation through Nox2 in *mdx* skeletal muscle.

Mdx skeletal muscle displays increased sarcolemmal Ca^{2+} influx in a redox dependent manner [4, 18]. We found that sarcolemmal Ca^{2+} influx was increased in quiescent unstretched *mdx* myofibers, which could be significantly attenuated with gp91 ds, PP2, or Rac1 inhibitor (Fig. 1h & Supplementary Figure 2a). Elevated intracellular Ca^{2+} is affiliated with excess RNS production in DMD pathology [19]. RNS production, which was significantly higher in myofibers from *mdx* mice compared to WT, was significantly attenuated by incubation with gp91 ds, PP2 or Rac1 inhibitor (Fig. 1i & Supplementary Figure 2b). These results demonstrate that Src kinase is a key regulator of Nox2 activity, leading to increased oxidative stress and Ca^{2+}- dependent RNS production in *mdx* skeletal muscle.

Src kinase regulates mTOR-dependent autophagy in *mdx* muscle

Autophagy is an evolutionary conserved cellular degradation pathway that contributes to cellular homeostasis and survival by degrading proteins and other cellular constituents. While a role for Src kinase in autophagy impairment has been reported in cancer pathogenesis [12], the mechanism for impaired autophagy in dystrophic muscle has not been elucidated. Immunoblot analyses showed that phospho-mTOR and phospho-Src levels were significantly increased in *mdx* skeletal muscle compared to WT (Fig. 1j), consistent with a block of autophagy. Accordingly, the levels of the autophagosomal membrane protein, sequestosome-1 (p62), were dramatically increased in *mdx* skeletal muscle (Fig. 1j). Examination of microtubule-associated protein-1 light chain 3 (LC3) showed a prevalence for the lipidated form (LC3II) in WT muscle (Fig. 1j), indicating the active formation of autophagic vesicles that were readily detected by confocal microscopy (Fig. 1k). Strikingly, *mdx* muscle was found to have attenuated LC3II levels (Fig. 1j) and to be devoid of LC3II-positive vesicles (Fig. 1k), indicating dramatic impairment of autophagic flux. Inhibition of Src kinase with PP2 decreased phospho-mTOR and phospho-Src in *mdx* skeletal muscle, with no change in total protein content (Fig. 1j). In addition, a concomitant increase in the ratio of LC3II to LC3I and a decrease in p62 protein levels were observed upon Src inhibition (Fig. 1j), providing further evidence for Src-dependent regulation of autophagic flux in *mdx* skeletal muscle. Importantly, inhibition of Src kinase restored the formation of LC3II-positive autophagic vesicles (Fig. 1k). p62, a marker of protein turnover, binds with LC3 and polyubiquitylated proteins, serving as a cargo receptor for the autolysosome degradation process [20]. Immunofluorecence analysis showed a marked decrease in p62 and autophagosome (LC3II) fusion (p62-LC3-positive puncta, yellow), a crucial event in autophagosome clearance, in *mdx* muscle compared to WT, which was dramatically rescued upon PP2 incubation (Fig. 1l). Together, these data suggest that activated Src kinase leads to a block of autophagy in *mdx* skeletal muscle.

Nox2/Src inhibition rescues autophagy in *mdx* mice

A rescue of autophagy induction obtained by inhibiting Src indicated that autophagy is not inherently compromised in *mdx* muscle. Thus, we investigated the potential downstream signaling pathway associated with autophagy blockage in order to identify possible therapeutic targets. Because the PI3K (type I)/Akt/mTOR/p70S6K axis is a primary regulatory pathway by which autophagy is suppressed, we asked whether impaired autophagy was dependent upon the exuberant activation of Nox2 in *mdx* muscle. Inhibition of Nox2 with gp91 ds reduced phosphorylation of Src (Y416), PI3K (Y458), Akt (T308) and mTOR (S2448) (Fig. 2a). Likewise, the level of phospho-S6 ribosomal protein (S235/236), a substrate of p70S6K and an indicator of p70S6K activity, also decreased (Fig. 2a). No significant changes were observed in WT muscle for any of these signaling molecules (Fig. 2a). Given that Nox2 inhibition decreased the phosphorylation of mTOR in *mdx* muscle, we then investigated autophagic flux. We found a highly significant decrease in p62-LC3 co-localization (yellow puncta) in flexor digitorum brevis (FDB) muscles from *mdx* mice compared to WT mice (Fig. 2b). Inhibition of Nox2 showed a marked recovery in p62-LC3 localization in mdx myofibers (Fig. 2b) in conjunction with a higher conversion of LC3I to LC3II, as well as a decrease in p62 protein levels in *mdx* muscle (Fig. 2c). Together, these

results demonstrate that inhibition of the Nox2/Src cycle induces mTOR-dependent autophagy.

Since autophagic flux appears to be suppressed in *mdx* muscle, we investigated whether there was an alteration in autophagosome formation. Colocalization of LC3 and LAMP1 was observed in WT myofibers, with no significant change upon inhibition of Nox2 or Src (Fig. 2d). *Mdx* myofibers showed a highly significant decrease in LC3-LAMP1-positive puncta, which were increased upon inhibition of either Nox2 or Src (Fig. 2d), thus confirming a blockage in autophagosome formation. We also observed a significant decrease in LAMP1 expression in *mdx* myofibers compared to WT, which was markedly restored upon inhibition of Nox2 or Src kinase (Fig. 2e). qPCR analysis of mRNA extracted from WT and *mdx* FDBs showed around a 33% decrease in LAMP1 transcript in *mdx* compared to WT (Supplementary Figure 3). These results suggest that increased oxidative stress may be a key regulatory factor of lysosomal maturation in *mdx* skeletal muscle.

Impaired autophagy is associated with aggregation of proteins and other cellular constituents, eventually leading to cell degeneration. Therefore, we investigated whether impaired autophagy in *mdx* muscle could lead to cell death. We found a marked increase in the apoptotic markers, poly [ADP-ribose] polymerase 1 (PARP-1) and cleaved caspase3, in *mdx* muscle compared to WT, which was significantly reduced upon inhibition of Src kinase activity (Fig. 2f). *Mdx* fibers incubated with rapamycin (an mTOR inhibitor) also showed a decrease in the cleavage of apoptotic markers (Fig. 2f). Inhibition of Nox2 activity led to a significant decrease in caspase3 cleavage (Fig. 2g). Taken together, our data demonstrate that the Nox2 complex plays a major role in impaired autophagy and muscle degeneration in *mdx* mice. Inhibition of Nox2-activity may lead to a decrease in cell degeneration by restoring autophagy.

Decreased Nox2 ROS and rescued autophagy in p47$^{-/-}$-*mdx* mice

Having established Nox2 and Src kinase as key upstream regulators of impaired autophagy in *mdx* skeletal muscle using pharmacological inhibitors, we next took a genetic approach to corroborate our findings. Genetic knock-out of p47^{phox} attenuates ROS generation in skeletal muscle [17]. Therefore, we hypothesized that genetic abrogation of p47^{phox} function in *mdx* mice would be beneficial against oxidative stress-induced damage. In muscle from mice deficient in p47^{phox} and dystrophin (p47$^{-/-}$-*mdx*) we found a highly significant reduction in ROS generation and Ca^{2+} influx (Fig. 3a&b), as well as a marked decrease in phosphorylation of Src kinase (Fig. 3c) compared to *mdx*. Reduced phosphorylation of mTOR, a significant increase in LC3I to LC3II conversion, and a concomitant decrease in p62 expression levels were evident in FDBs from p47$^{-/-}$-*mdx* mice compared to *mdx* (Fig. 3d), indicating enhanced autophagic flux in p47$^{-/-}$-*mdx* compared to *mdx*. Treatment of myofibers with rapamycin increased LC3II to LC3I ratios and decreased p62 and phospho-mTOR levels in mdx myofibers (Fig. 3d). We also found a rescue in LAMP1 protein expression and fusion of LC3 and LAMP1-positive vesicles in p47$^{-/-}$- *mdx* mice compared to *mdx* mice (Fig. 3e). Rescue of autophagy was also observed in tibialis anterior (TA), diaphragm (Dia) and soleus (Sol) skeletal muscles of p47$^{-/-}$-*mdx* mice (Supplementary

Figure 4a-c). Thus, inhibition of Nox2-activity rescues *mdx* muscle from oxidative stress and subsequently maintains the homeostasis of the autophagic machinery.

p47$^{-/-}$-*mdx* mice show significant rescue in lysosomal biogenesis

Because autophagy is a lysosome-dependent process, we next investigated the status of lysosomal biogenesis in *mdx* muscle. Both immunofluorescence (Fig. 3f) and immunohistochemical assays (Fig. 3g) showed a marked decrease in lysosome formation in *mdx* muscle compared to WT, indicating that exuberant activation of Nox2 and Src kinase impairs lysosome biogenesis. Interestingly, analysis of p47$^{-/-}$-*mdx* muscle showed rescue of lysosomal biogenesis compared to *mdx* (Fig. 3f-g) These results identify the lysosomalautophagy pathway as a critical and reversible point of intersection among pathways that are dysregulated in the cellular pathogenesis of DMD.

Improved pathophysiological abnormalities in p47$^{-/-}$-mdx

Since genetic ablation of p47^{phox} rescued *mdx* muscle from excess ROS production, exuberant sarcolemmal Ca^{2+} influx, and defective autophagy-lysosomal function, we next investigated whether these changes improved the pathological abnormalities and contractile dysfunction of *mdx* skeletal muscle. Hematoxylin and eosin (H&E) staining revealed decreased cross-sectional area (292 μm^2 vs. 470 μm^2) and increased centronucleated myofibers (57% vs. 5%) in *mdx* diaphragm, compared to WT (Fig 4a), both hallmarks of the dystrophic phenotype. Diaphragm muscle from p47$^{-/-}$-*mdx* mice showed a decrease in the number of centronucleoted myofibers (30%) and a shift in the cross-sectional area (521 μm^2) to larger fibers, similar to WT (Fig 4a). TA from *mdx* mice showed a significant increase in immune cell infiltration compared to WT, which was markedly decreased in p47$^{-/-}$-*mdx* mice (Fig. 4b). We found that ablation of p47^{phox} in *mdx* skeletal muscle prevented the IIB to IIA fiber-type switch that occurs in mdx skeletal muscle (Fig 4c). In *mdx* mice serum creatine kinase was 37.5 fold higher than WT. There was a trend for a decrease (22.6%) in serum creatine kinase activity in p47$^{-/-}$-*mdx* mice compared to *mdx*; however, it did not reach statistical significance (Fig 4d). Importantly, we also found that diaphragm muscle from p47$^{-/-}$-*mdx* mice had greatly improved functional properties compared to diaphragm from *mdx* mice (Fig 4e). Both twitch and tetanic forces were significantly lower in *mdx* diaphragm compared to WT (41% and 49%, respectively). Genetic down regulation of Nox2 significantly improved both twitch (50%) and tetanic (31%) force production in diaphragm from p47$^{-/-}$-*mdx* compared to *mdx*. Taken together, our results show that down regulation of the Nox2/Src pathway improves the pathological and functional defects of dystrophic skeletal muscle by upregulating the autophagy-lysosome system.

Discussion

Previous work has reported upregulation of Nox2 content prior to an increase in immune cell infiltration [4]. The signaling pathways modified by Nox2-dependent ROS, however, have not been identified. Increased activation of mTOR [21] and impaired autophagy have been observed in *mdx* skeletal muscle [9, 22]. While treatment of *mdx* mice with rapamycin (an mTOR inhibitor) [21] or a prolonged low-protein diet [9] were able to reduce muscle inflammation, necrosis, and muscle damage, the mechanisms leading to defective autophagy

and the potential upstream regulatory pathways were not investigated. In this study we establish, for the first time, a mechanism by which Nox2-specific oxidative stress impairs autophagy, through Src kinase-dependent activation of the PI3K/Akt/mTOR pathway. Furthermore, we discovered that lysosome formation is defective in *mdx* skeletal muscle (Fig. 5). Proper lysosome formation is necessary for recycling of molecules and nutrients as well as to rid the cell of unwanted or damaged organelles. The severe decrease in lysosomal biogenesis in *mdx* mice may lead to the failure in starvation-dependent activation of autophagy in *mdx* mice [9]. Pharmacological or genetic inhibition of Nox2 reactivated autophagy, rescued lysosomal biogenesis, and rescued the pathological as well as the physiological phenotype of dystrophic skeletal muscle. Our data indicate that pharmacological or genetic inhibition of Nox2 or Src kinase may prove to be beneficial therapeutic targets for the treatment of DMD.

Using our targeted redox biosensor p47-roGFP [17], we established that the Nox2-complex is a significant source of oxidative stress in *mdx* skeletal muscle. Nox2-dependent ROS production enhanced Ca^{2+} influx and generation of RNS, as well as activated Src kinase, which in turn leads to further activation of Nox2 via $p47^{phox}$ phosphorylation. Although we cannot exclude the involvement of other ROS sources (i.e. mitochondria), inhibition of the Nox2-complex and Src kinase significantly reduced oxidative stress in *mdx* muscle.

Autophagy is a dynamic cellular pathway involved in maintenance of cellular homeostasis by degradation of misfolded/toxic proteins and other damaged cellular constituents [23]. Impaired autophagic flux is detrimental to skeletal muscle and plays a major role in the pathology of several skeletal muscle disorders [11, 24]. We found a significant enhancement in phosphorylated Src and reduction in the lipidated form of LC3 (LC3II) in muscle fibers from *mdx* mice. Reduction of LC3II protein and LC3 positive puncta was accompanied by enhanced presence of phosphorylated mTOR and increased levels of p62, all of which support a decrease in autophagic flux in *mdx* skeletal muscle. Inhibition of either Nox2 or Src kinase in *mdx* skeletal muscle was able to inhibit the PI3K/Akt/mTOR pathway, decrease p62 levels and restore LC3II levels. Inhibition of autophagy can lead to degeneration of skeletal muscle [25]. In agreement with previous reports, we found increased apoptotsis in muscle fibers from *mdx* mice compared to WT mice, which could be partially attenuated by inhibition of Nox2 or Src kinase. These findings support our hypothesis that Nox2 and Src kinase are key regulatory factors in defective autophagic machinery in *mdx* muscle.

Our data appear to be contrary to evidence in the literature which support a role for ROS induced autophagy, for review see [26, 27]. Huang et al [28] report that Nox2 derived ROS is important for autophagy induction in phagocytic cells while here we show that Nox2 ROS impairs autophagy. This dichotomy may lie in the spatial and temporal production of ROS. ROS participate in cellular signaling; however, when produced at high levels or for extended periods of time they can cause irreversible oxidative damage. Dystrophic skeletal muscle is under constant oxidative stress. In addition, the subcellular localization of Nox2 with Src kinase in caveolae within the skeletal muscle sarcolemma [4, 6] may provide a spatially privileged communication, allowing Nox2-dependent ROS to activate Src and the PI3K/Akt/mTOR pathway and thereby inhibit autophagy.

Late autophagy is marked by autophagosome coalescence and fusion with lysosomes to form autolysosomes. It has been reported that elevated oxidative stress is associated with decreased LAMP1 expression and impaired lysosomal maturation [29]. Muscle fibers from *mdx* mice contain a marked decrease in LC3/LAMP1 autolysosome positive structures and a significant reduction in the expression of LAMP1, which can be restored with pharmacological or genetic inhibition of Nox2-specific oxidative stress. Further, we saw a significant decrease in lysosome coalescence in *mdx* muscle. Lysosomes have long been identified as participating in signaling pathways that sense nutrient deprivation and facilitate energy metabolism by inducing autophagy in response to starvation [30]. Clementi and colleagues have reported a failure in activation of autophagy in *mdx* mice in response to starvation [9]. In this study, we found severe damage in lysosomal biogenesis in *mdx* mice, suggesting that lack of lysosome formation may lead to failure of starvation-dependent activation of autophagy in *mdx* mice. These finding indicate that DMD may be characterized as a lysosomal dysfunctional disorder. Transcriptional behavior and functional integrity of most of the lysosomal genes are regulated by transcription factor EB (TFEB) [31]. While oxidative stress has been suggested to down-regulate functional activity of TFEB and lysosomal activity [32], the specific mechanisms of action have yet to be established. We are currently investigating the regulatory mechanisms of TFEB in transcription of LAMP1 in *mdx* skeletal muscle.

To investigate the role of Nox2/Src kinase-dependent impairment of autophagy in the pathophysiology of DMD, we assessed several histopathological markers and muscle function upon genetic down regulation of Nox2 activity. In the *mdx* mouse muscle infiltration of immune cells is recognized by 3-4 weeks of age, followed by massive degeneration/necrosis, elevated serum creatine kinase activity, and replacement of muscle with fibrosis and fatty tissue at around 12 weeks of age. In our studies we observed significant improvement of the pathophysiological phenotype of diaphragm muscle from young (4-6 weeks) $p47^{-/-}$-*mdx* mice, an age prior to replacement of muscle fibers with fibrotic and fatty tissue, as evidenced by prevention of IIB to IIA fiber type switch, maintenance of cross-sectional area, and percent fibers with central nuclei, and reduced immune cell infiltration. Consistent with previous reports, we found a significant increase in serum creatine kinase levels in *mdx* mice compared to WT mice. However, $p47^{-/-}$-*mdx* mice did not show a significant reduction serum creatine kinase levels compared to *mdx* mice. Creatine kinase can be released from the muscle in response to fiber damage, degeneration/regeneration, or necrosis. We found a significant decrease in apoptosis in muscle from $p47^{-/-}$-*mdx* mice and protection against a decline in force production in diaphragm muscle, thus the elevated serum CK levels in the $p47^{-/-}$-*mdx* mice may be due to some persistent ongoing degeneration/regeneration. In the *mdx* mouse the diaphragm is the most severely dystrophic skeletal muscle and best represents the progression of the human disease. Since respiratory failure is a leading cause of death in DMD, rescuing the functional deficits in dystrophic diaphragm will improve respiratory function and therefore quality of life for patients suffering from DMD.

In conclusion, this study demonstrates the presence of a Nox2/Src kinase-dependent impairment of autophagy in *mdx* skeletal muscle. Both pharmacological and genetic

inhibition of Nox2 or Src kinase led to restoration of the autophagic machinery and improvement of the pathophysiological phenotype. As Nox2 and Src kinase are upregulated early in the progression of the disease, prior to muscle damage and inflammation, Nox2/Src may prove to be beneficial therapeutic targets for the treatment of DMD. Targeting Src kinase is of particular interest, as Src kinase inhibitors are currently in Phase II clinical trials for the treatment of certain types of cancer. Additional preclinical studies are currently underway in our laboratory to assess the efficacy of in vivo Src inhibitors on the pathophysiology of dystrophic muscle.

Methods

Chemical reagents and antibodies

PP2 was purchased from Calbiochem. Rapamycin, pegylated-catalase (PEG-cat), catalase (Cat), N-Acetyl Cysteine (NAC), and ECM gel (from Engelbreth-Holm-Swarm murine sarcoma) were purchased from Sigma-Aldrich. Fura-2/AM, DAF-FM, Amplex-red and DCFH-DA (6-carboxy-2′,7′-dichlorodihydrofluorescein diacetate) were from Invitrogen. The Nox-specific peptide inhibitor gp91 ds were from Biosynthesis, Lewisville, TX. Anti-Src, anti-P-Src, anti-PI3K, anti-P-PI3K, anti-Akt, anti-P-Akt, anti-mTOR, anti-P-mTOR, anti-p70S6K, anti-P-p70S6K, anti-S6, anti-P-S6, anti-caspase3, anti-Cleaved-caspase3, anti-LC3B, anti-PARP1 and anti-LAMP1 antibodies were from Cell Signaling Technology. Anti-GAPDH (glyceraldehyde-3-phosphate dehydrogenase), anti-active Rac1, anti-$p47^{phox}$ and anti-P-serine were purchased from Millipore. Anti-Type I (BA-F8) and anti-Type IIA (SC-71) were purchased from Developmental Studies Hybridoma Bank (DSHB). IgG1 and IgG2b isotype-specific secondary antibodies were purchased from Invitrogen. Anti-p62 and Protein G PLUS-Agarose were from Santacruz Biotechnologies. Anti-Rac1 was from Abcam. ODYSSEY secondary antibodies for western blot (anti-mouse*680*, anti-mouse*800*, anti-rabbit*680*, anti-rabbit*800* and anti-goat*800*) were purchased from LI-COR Biosciences. Secondary antibodies for immunofluorescence (Alexa Fluor® 488 Chicken-anti-mouse and Alexa Fluor® 594 Donkey-anti-rabbit) were purchased from Invitrogen. DMEM was from Gibco, heat inactivated fetal bovine serum (FBS) was purchased from Atlanta Biologicals. 96-well plates were from Costar, X-tremeGENE HP DNA Transfection Reagent and Collagenase A was from Roche Applied Science. Detailed information about antibodies and dilution can be found in Supplementary Table 1.

Generation of $p47^{phox}$-dystrophin double knock-out animals

Male homozygous mice lacking $p47^{phox}$ (B6(Cg)-*Ncf1*^{m1J}/J, JaxMice) were crossed with female homozygous dystrophic deficient mice C57BL/10ScSn-*Dmd*^{mdx}/J, JaxMice) to generate $p47^{phox+/-}$-$dystrophin^{+/-}$ mice. Male and female siblings were mated to generate $p47^{phox-/-}$ -$dystrophin^{-/-}$female mice. Female $p47^{phox-/-}$ - $dystrophin^{-/-}$ mice were back-crossed with $p47^{phox-/-}$males to generate $p47^{phox-/-}$ - $dystrophin^{+/-}$ females. These $p47^{phox-/-}$ - $dystrophin^{+/-}$ female mice were back-crossed into $p47^{phox-/-}$ males for at least 6 generations to obtain mice on a C57BL6/J background.

Isolation of FDB fibers and treatment

Mice were deeply anesthetized by isoflurane (2%) inhalation and euthanized by rapid cervical dislocation in accordance with National Institutes of Health guidelines and approved by the Institutional Animal Care and Use Committee of Baylor College of Medicine. Flexor digitorum brevis (FDB) muscles were surgically isolated and incubated in minimal essential media containing 0.1% gentamycin and 0.4% Collagenase A at 37°C for 1.5–2.0 h. To release single fibers, FDB muscles were then triturated gently in serum containing media (10%, Atlanta Biologicals) without collagenase and incubated in 5% CO_2 at 37°C until used, typically 12–36 h later. All other muscles were rapidly frozen in liquid nitrogen and stored at −80°C until used.

For western blotting and immunostaining, fibers were treated with PP2 (0.2 μM) or gp91 ds (5 μM) at 37°C for 24 h. For all other experiments, fibers were incubated with PP2 (0.2 μM), gp91 ds (5 μM) or Rac1 inhibitor (50 μM) at 37°Cfor 2 h.

ROS measurements

Enzymatically digested single FDBs were seeded on 96-well plates for either intracellular (DCFH-DA) or extracellular (Amplex-red) ROS measurements. DCF fluorescence was excited at 480 nm via a Sutter Lamda DG-5 Ultra high speed wavelength switcher, and emission intensity was collected at 510 nm at a rate of 0.1 Hz. Amplex red dye was excited at 550 nm via a Sutter Lamda DG-5 Ultra high speed wavelength switcher, and emission intensity was collected at 590 nm at a rate of 0.1 Hz. For assessment of Nox2 activity and glutathione redox potential (oxidative stress) FDBs were electroporated with either p47-roGFP or Grx1-roGFP2, respectively and fluorescence ratios quantified as previously described [17, 33].

Assessment of Ca^{2+} influx by Mn^{2+} quench and RNS measurement

Calcium influx was assessed using the Mn^{2+} quench of Fura-2 fluorescence as previously reported [3, 34]. RNS was measured using DAF-FM dye. Excitation was at 488 nm and emission was captured with a linear detector after passing through a 495-555 nm band pass filter.

Westernblotting

Lysates from either enzymatically digested FDBs or whole tissue (diaphragm, tibialis anterior, soleus, extensor digitorum longus) were extracted and quantified with the bicinchoninic acid (BCA) protein assay kit (Pierce, Rockford, IL), using BSA as standard. Lysates were separated via SDS-PAGE and then transferred to polyvinyldifluoride (PVDF) membranes. Blots were incubated in blocking buffer (5%, w/v, dried skimmed milk in Tris-buffered saline, pH 7.4, and 0.2% Tween 20, TBST) followed by overnight incubation with appropriate antibodies diluted in blocking buffer (5% BSA in TBST). Blots were then exposed to the IRDye® Secondary Antibodies (LI-COR) diluted in TBST for 60 min at room temperature and washed again. Blots were detected using LI-COr® Odyssey Infrared Imaging System and analyzed using ImageJ software. Representative uncropped blots are shown in Supplementary Figure 5.

Immunoprecipitation of p47^{phox}

For p47^{phox} immunoprecipitation, enzymatically digested FDB fibers were incubated in the absence and presence of gp91 ds or PP2 and the cytosolic fraction (100 μg protein) was transferred to microcentrifuge tubes, and anti-p47^{phox} antibody (15 μg) was added and incubated for 60 minutes at 4°C. Agarose conjugate (30 μL, Protein G PLUS-Agarose) was added and incubated (60 minutes, 4°C). Samples were centrifuged, and the supernatant was subjected to immunoblotting and probed with anti-phosphoserine antibody and anti-p47^{phox} antibodies.

Assessment of autophagy by immunostaining

FDB muscles were removed immediately after sacrifice and cultured overnight with or without treatment. On the day of experiments, fibers were plated on ECM gel from Engelbreth-Holm-Swarm murine sarcoma (Sigma, St. Louis, MO) coated glass-bottom culture dishes for 1 h. Fibers were then fixed with 4% paraformaldehyde in 0.1 M phosphate buffer (PBS) for 15 min. Fibers were blocked with blocking reagent (0.1% saponin, 8% goat serum in PBS) for 1 h. The fibers were then permeabilized with 0.1% triton, incubated with primary antibody (LC3 and LAMP1) for overnight at 4°C, washed, incubated with secondary antibodies for 2 h, and washed again prior to microscopy.

Histology and serum creatine kinase activity

Serial sections of 12 μm thickness were cut from the mid-belly region of diaphragm and tibialis anterior (TA) muscles on a refrigerated cryostat (Shandon Cryotome E, Thermo) at −20°C. Sections were stained with hematoxylin and eosin (H&E) and Masson'sTrichrome. Digitized images (8 bit) of muscle sections were acquired with a CCD camera (Digital Sight DSFi1, Nikon) attached to an upright microscope (Nikon Eclipse 80i). Images were analyzed with NIS Elements Br software (Nikon) where the mean cross sectional area (CSA) of muscle fibers was calculated by interactive determination of the circumference of at least 200 adjacent cells from the center of every muscle section examined. Percentage of central nuclei was determined from at least 200 fibers from at least 3 mice of each genotype. For serum creatine kinase (CK) activity blood was drawn from the saphenous vein, serum separated and CK activity measured on a Cobas Integra 400/800 analyzer (Roche).

Immunofluorescence and immunohistochemistry

Serial sections of 6-12 μm thickness were fixed with cold methanol for 20 min. For immunofluorescence, frozen tissue sections were incubated overnight with appropriate antibodies in a humid box at 4°C followed by incubation with appropriate secondary antibody [1:300] for 3 hours. Slides were then mounted with vectashield containing DAPI (H-1200). For the immunohistochemistry, frozen sections were incubated with 0.3% H_2O_2 solution in PBS at room temperature for 20 min to quench endogenous peroxidase activity and incubated with the primary antibody overnight at 4°C in a humid box. The sections were then subjected to the secondary antibody from the VECTASTAIN Elite ABC kit (Vector Lab) according to the manufacturer's instructions. The slides were developed with DAB substrate kit (SK-4100).

Real-time PCR

Total RNA was extracted from FDBs of wt and mdx mice by using a miRNeasy Mini kit (Qiagen), and 1 mg of total RNA was used to synthesize cDNA by Quantitect reverse transcription kit (Qiagen). Real-time quantitative RT-PCR on cDNAs was carried out with the iTaq Universal SYBR Green Supermix (Biorad) using the CFX96 real time PCR detection system (Biorad) with the following conditions: 95°C, 5 min; (95°C, 10 s; 60°C, 10 s; 72°C, 15 s) × 40. For expression studies the qRT-PCR results were normalized against an internal control (Cyclophillin). Oligonucleotide sequences were: Lamp1-F (5′-CCTACGAGACTGCGAATGGT-3′) Lamp1-R (5′- CCACAAGAACTGCCATTTTTC-3′) Cyclophilin-F (5′- GGCAAATGCTGGACCAAACACAA-3′) Cyclophilin-R (5′-GTAAAATGCCCGCAAGTCAAAAG-3′).

Ex vivo force measurements

Diaphragm muscle was dissected from mice and one end tied to a fixed hook and the other to a force transducer (F30, Harvard Apparatus) using silk suture (4-0) in a physiological saline solution continuously gassed with 95% O_2–5% CO_2 at 30°C. Contractile properties were assessed by passing a current between two platinum electrodes at supra-maximal voltage (PanLab LE 12406, Harvard Apparatus) with pulse and train durations of 0.25 and 400ms, respectively. Muscle length was adjusted to elicit maximum twitch force (optimal length, Lo) and the muscle was allowed a 15 minute equilibration period. To define the force-frequency characteristics force was measured at stimulation frequencies of 1, 5, 10, 20, 40, 60, 80, 120, 150 and 200-Hz every 1 minute. At the end of the contractile protocol muscle length was measured using a hand-held electronic caliper, fiber bundles removed from the organ bath and trimmed of excess bone and connective tissue, blotted dry, and weighed. Muscle weight and Lo was used to estimate cross-sectional area and absolute forces expressed as N/cm^2 [35]

Data Analysis

Data are reported as mean ± SEM, unless otherwise specified. Statistical differences between groups were determined using ANOVA with Tukey's post-hoc test. Statistical analysis was performed in Origin Pro (OriginLab Corporation, Northhampton, MA) with a significance level of $*p < 0.05$ and $**p<0.01$. Colocalization analysis in single fibers was done in ImageJ.

Supplementary Material

Refer to Web version on PubMed Central for supplementary material.

Acknowledgement

We thank K. Ma for critical discussions. Research reported in this publication was supported by the National Institute of Neurological Disorders and Stroke of the National Institutes of Health under Award Number R01 NS079618 to M.S. The National Institute of Arthritis and Musculoskeletal and Skin Diseases of the National Institutes of Health under Award Number R01 AR061370, a Mrs. Clifford Elder White Graham Endowed Research Fund Award, and a Gillson Longenbaugh Foundation Award to G. G. R. The content is solely the responsibility of the authors and does not necessarily represent the official views of the National Institutes of Health

Reference List

1. Hoffman EP, Brown J, Kunkel LM. Dystrophin: The protein product of the duchenne muscular dystrophy locus. Cell. 1987; 51:919–928. [PubMed: 3319190]
2. van Deutekom JC, van Ommen GJ. Advances in Duchenne muscular dystrophy gene therapy. Nat. Rev. Genet. 2003; 4:774–783. [PubMed: 14526374]
3. Mariol MC, Segalat L. Muscular degeneration in the absence of dystrophin is a calcium-dependent process. Current Biology. 2001; 11:1691–1694. [PubMed: 11696327]
4. Whitehead NP, Yeung EW, Froehner SC, Allen DG. Skeletal muscle NADPH oxidase is increased and triggers stretch-induced damage in the mdx mouse. PLoS. One. 2010; 20;5:e15354.
5. Prosser BL, Khairallah RJ, Ziman AP, Ward CW, Lederer WJ. X-ROS signaling in the heart and skeletal muscle: Stretch-dependent local ROS regulates $[Ca^{2+}]_i$. Journal of Molecular and Cellular Cardiology. 2013; 58:172–181. [PubMed: 23220288]
6. Gervasio OL, Whitehead NP, Yeung EW, Phillips WD, Allen DG. TRPC1 binds to caveolin-3 and is regulated by Src kinase - role in Duchenne muscular dystrophy. J Cell Sci. 2008; 121:2246–2255. [PubMed: 18544631]
7. Touyz RM, Yao G, Schiffrin EL. c-Src induces phosphorylation and translocation of p47phox: role in superoxide generation by angiotensin II in human vascular smooth muscle cells. Arterioscler. Thromb. Vasc. Biol. 2003; 23:981–987. [PubMed: 12663375]
8. Dalloz C, et al. Targeted inactivation of dystrophin gene product Dp71: phenotypic impact in mouse retina. Hum. Mol. Genet. 2003; 12:1543–1554. [PubMed: 12812982]
9. De Palma C, et al. Autophagy as a new therapeutic target in Duchenne muscular dystrophy. Cell Death. Dis. 2012; 3:e418:e418. [PubMed: 23152054]
10. Bernardi P, Bonaldo P. Mitochondrial dysfunction and defective autophagy in the pathogenesis of collagen VI muscular dystrophies. Cold Spring Harb. Perspect. Biol. 2013; 5:a011387. [PubMed: 23580791]
11. Grumati P, et al. Autophagy is defective in collagen VI muscular dystrophies, and its reactivation rescues myofiber degeneration. Nat. Med. 2010; 16:1313–1320. [PubMed: 21037586]
12. Wu Z, et al. Autophagy Blockade Sensitizes Prostate Cancer Cells towards Src Family Kinase Inhibitors. Genes Cancer. 2010; 1:40–49. [PubMed: 20811583]
13. Haynes MP, et al. Src kinase mediates phosphatidylinositol 3-kinase/Akt-dependent rapid endothelial nitric-oxide synthase activation by estrogen. J. Biol. Chem. 2003; 278:2118–2123. [PubMed: 12431978]
14. Katz S, Ayala V, Santillan G, Boland R. Activation of the PI3K/Akt signaling pathway through P2Y(2) receptors by extracellular ATP is involved in osteoblastic cell proliferation. Arch. Biochem. Biophys. 2011; 513:144–152. [PubMed: 21763267]
15. Chen S, et al. IBP-mediated suppression of autophagy promotes growth and metastasis of breast cancer cells via activating mTORC2/Akt/FOXO3a signaling pathway. Cell Death. Dis. 2013; 4:e842:e842. [PubMed: 24113176]
16. Walker CL, et al. Systemic bisperoxovanadium activates Akt/mTOR, reduces autophagy, and enhances recovery following cervical spinal cord injury. PLoS. One. 2012; 7:e30012. [PubMed: 22253859]
17. Pal R, Basu TP, Li S, Minard C, Rodney GG. Real-time imaging of NADPH oxidase activity in living cells using a novel fluorescent protein reporter. PLoS. One. 2013; 8:e63989. [PubMed: 23704967]
18. Khairallah RJ, et al. Microtubules Underlie Dysfunction in Duchenne Muscular Dystrophy. Sci. Signal. 2012; 5:ra56. [PubMed: 22871609]
19. Altamirano F, et al. Increased resting intracellular calcium modulates NF-kappaB-dependent inducible nitric-oxide synthase gene expression in dystrophic mdx skeletal myotubes. J. Biol. Chem. 2012; 287:20876–20887. [PubMed: 22549782]
20. Lichtenstein A, Minogue PJ, Beyer EC, Berthoud VM. Autophagy: a pathway that contributes to connexin degradation. J. Cell Sci. 2011; 124:910–920. [PubMed: 21378309]

21. Eghtesad S, Jhunjhunwala S, Little SR, Clemens PR. Rapamycin ameliorates dystrophic phenotype in mdx mouse skeletal muscle. Mol. Med. 2011; 17:917–924. [PubMed: 21607286]
22. Spitali P, et al. Autophagy is Impaired in the Tibialis Anterior of Dystrophin Null Mice. PLoS. Curr. 2013; 5 pii: ecurrents.md.e1226cefa851a2f079bbc406c0a21e80., ecurrents.
23. Nixon RA. The role of autophagy in neurodegenerative disease. Nat. Med. 2013; 19:983–997. [PubMed: 23921753]
24. Sandri M, Coletto L, Grumati P, Bonaldo P. Misregulation of autophagy and protein degradation systems in myopathies and muscular dystrophies. J. Cell Sci. 2013; 126:5325–5333. [PubMed: 24293330]
25. Masiero E, Sandri M. Autophagy inhibition induces atrophy and myopathy in adult skeletal muscles. Autophagy. 2010; 6:307–309. [PubMed: 20104028]
26. Lam GY, Huang J, Brumell JH. The many roles of NOX2 NADPH oxidase-derived ROS in immunity. Semin. Immunopathol. 2010; 32:415–430. [PubMed: 20803017]
27. Gibson SB. Investigating the role of reactive oxygen species in regulating autophagy. Methods Enzymol. 2013; 528:217–35. doi: 10.1016/B978-0-12-405881-1.00013-6., 217-235. [PubMed: 23849868]
28. Huang J, et al. Activation of antibacterial autophagy by NADPH oxidases. Proc. Natl. Acad. Sci. U. S. A. 2009; 106:6226–6231. [PubMed: 19339495]
29. Dehay B, et al. Pathogenic lysosomal depletion in Parkinson's disease. J. Neurosci. 2010; 30:12535–12544. [PubMed: 20844148]
30. Settembre C, Fraldi A, Medina DL, Ballabio A. Signals from the lysosome: a control centre for cellular clearance and energy metabolism. Nat. Rev. Mol. Cell Biol. 2013; 14:283–296. [PubMed: 23609508]
31. Sardiello M, et al. A gene network regulating lysosomal biogenesis and function. Science. 2009; 325:473–477. [PubMed: 19556463]
32. Porter K, Nallathambi J, Lin Y, Liton PB. Lysosomal basification and decreased autophagic flux in oxidatively stressed trabecular meshwork cells: implications for glaucoma pathogenesis. Autophagy. 2013; 9:581–594. [PubMed: 23360789]
33. Gutscher M, et al. Real-time imaging of the intracellular glutathione redox potential. Nat. Methods. 2008; 5:553–559. [PubMed: 18469822]
34. Pal R, Monroe TO, Palmieri M, Sardiello M, Rodney GG. Rotenone induces neurotoxicity through Rac1-dependent activation of NADPH oxidase in SHSY-5Y cells. FEBS Lett. 2013; 10
35. Close RI. Dynamic properties of mammalian skeletal muscles. Physiol Rev. 1972; 52:129–197. [PubMed: 4256989]

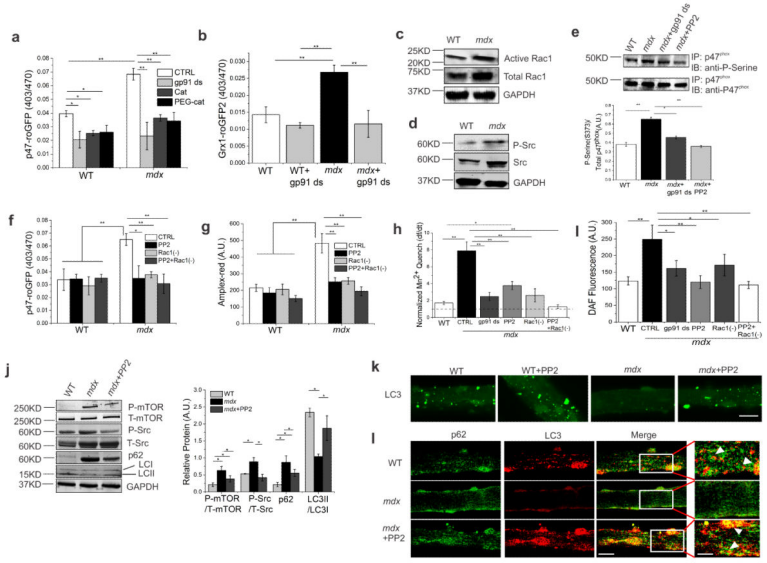

Figure 1. Inhibition of Nox2-activity reduces oxidative stress and Src kinase-mediated impaired autophagy

(**a**) Nox2-specific ROS production was assessed using the Nox2 redox biosensor p47-roGFP redox biosensor Cat: catalase, PEG-Cat: pegylated catalse. (**b**) Measurement of intracellular glutathione redox potential with Grx1-roGFP2. (**c**) Analysis of Rac1 and (**d**) Src. (**e**) Immunoblot of precipitated $p47^{phox}$ probed with an anti-phosphoserine or anti-$p47^{phox}$ antibody. (**f**) Nox2-specific intracellular ROS production was measured using p47-roGFP redox biosensor. (**g**) Extracellular ROS production was assessed using Amplex-red dye. (**h**) Plasma membrane calcium influx was measured by analyzing the Fura-2 fluorescence quench rate upon addition of extracellular Mn^{2+}. (**i**) Intracellular RNS generation was measured using DAF-FM. Bars represent average ±SEM from n=15 individual fibers for each condition in (**a**, **b**, **f**, **g**, **j** and **i**). Markers of autophagy were analyzed in isolated fibers (incubated with or without PP2) from FDBs. (**k**) Autophagosome formation was analyzed using fluorescence microscopy (scale bar=100 μm) and illustrated LC3 localization and autophagosome formation. (**l**) Confocal microscopy detected p62-LC3 localization in single fibers from FDBs (scale bar=140 μm and 50 μm for white box areas). All immunoblots were performed with isolated proteins from FDBs and probed with antibodies as indicated. GAPDH was detected as a loading control. Representative images are shown. Bars represent average ±SEM from n=3 independent biological experiments. Statistical differences between groups were determined using ANOVA with Tukey's post-hoc test. *$p < 0.05$ and **$p<0.01$.

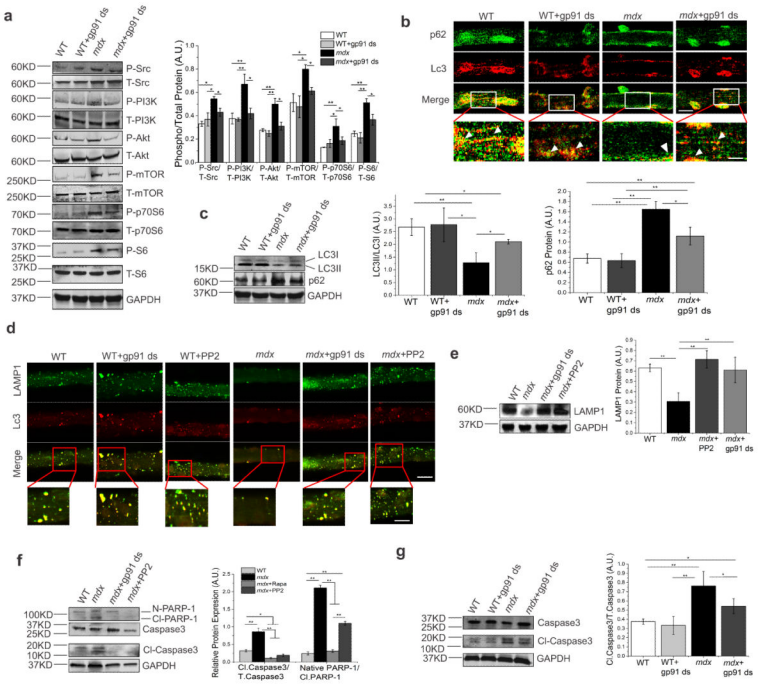

Figure 2. Inhibition of Nox2 and Src kinase induces autophagy and prevents cell degeneration in mdx mice via PI3K/Akt/mTOR pathway

(**a**) FDB lysates were analyzed by immunoblotting with antibodies as indicated. (**b**) Confocal microscopy shows the effect of Nox2 inhibition on p62-LC3 localization in single FDB fibers. Representative images of independent biological experiments (n=3) are shown (scale bar=100 μm and 35 μm for white box areas). **(c)** Autophagic flux was analyzed by immunoblotting with anti-LC3B and anti-p62 antibodies. (**d**) Effect of gp91 ds and PP2 on LC3-LAMP1 colocalization was analyzed by confocal microscopy. Representative images from independent biological experiments (n=3) are shown (scale bar=140 μm and 40 μm for red box areas). (**e**) Immunoblot analysis of LAMP1, (**f**) PARP-1 and caspase3 activity. (**g**) Immunoblot of Caspase3 activity. All immunoblots were performed with isolated proteins from FDBs and probed with antibodies as indicated. GAPDH was detected as a loading control. Representative images are shown. Bars represent average ±SEM from n=3 independent biological experiments. Statistical differences between groups were determined using ANOVA with Tukey's post-hoc test. *p < 0.05 and **p<0.01.

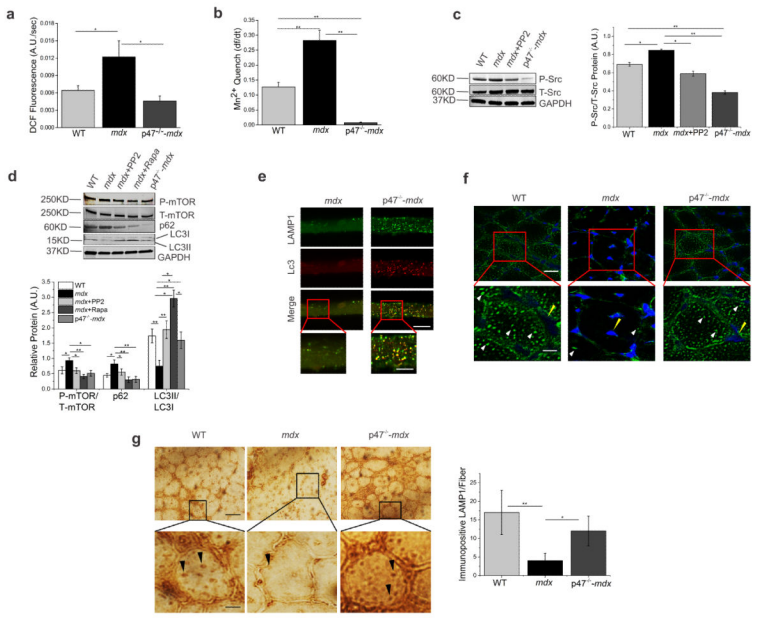

Figure 3. Genetic deletion of p47^{phox} decreases oxidative stress and induces activation of autophagy in *mdx* mice

(**a**) Intracellular ROS production was assessed using DCFH-DA. (**b**) Plasma membrane calcium influx was measured by analyzing the quench of Fura-2 fluorescence upon addition of extracellular Mn^{2+}. (**a**) and (**b**) were conducted in enzymatically digested single FDBs from WT, *mdx* and p47$^{-/-}$-*mdx* mice. Bars represent average ±SEM from n=15 individual fibers for each condition. (**c**) Immunoblot analysis of Src protein with anti-P-Src or anti-Src antibodies. (**d**) Autophagy marker proteins were analyzed by immunoblotting with antibodies as indicated (**c**) and (**d**) were conducted in enzymatically isolated fibers from FDBs of WT, *mdx* and p47$^{-/-}$-*mdx* mice. Representative images are shown. GAPDH was detected as a loading control. Bars represent average ±SEM from n=3 independent biological experiments. (**e**) LC3-LAMP1 colocalization in single FDBs from *mdx* and p47$^{-/-}$-*mdx* mice was analyzed by confocal microscopy. Representative images from n=3 independent biological experiments are shown (scale bar=100 μm and 40μm for red box areas). (**f**) Immunofluorescence assay to detect lysosomes (LAMP1) in TA muscle from WT, *mdx* and p47$^{-/-}$-*mdx* mice. White arrows indicate lysosome and yellow arrows indicate nucleus. (**g**) Immunohistochemistry to detect lysosome (LAMP1) in TA muscle from WT, *mdx* and p47$^{-/-}$-*mdx* mice. Black arrows indicate LAMP1 positive (brown) structures. Histogram plot quantifying the number of immunopositive LAMP1 structures per fiber. Representative images from n=3 independent biological experiments are shown. Scale bar represents 100 μm for **f** and 140 μm for **g**. Statistical differences between groups were determined using ANOVA with Tukey's post-hoc test. *p < 0.05 and **p<0.01.

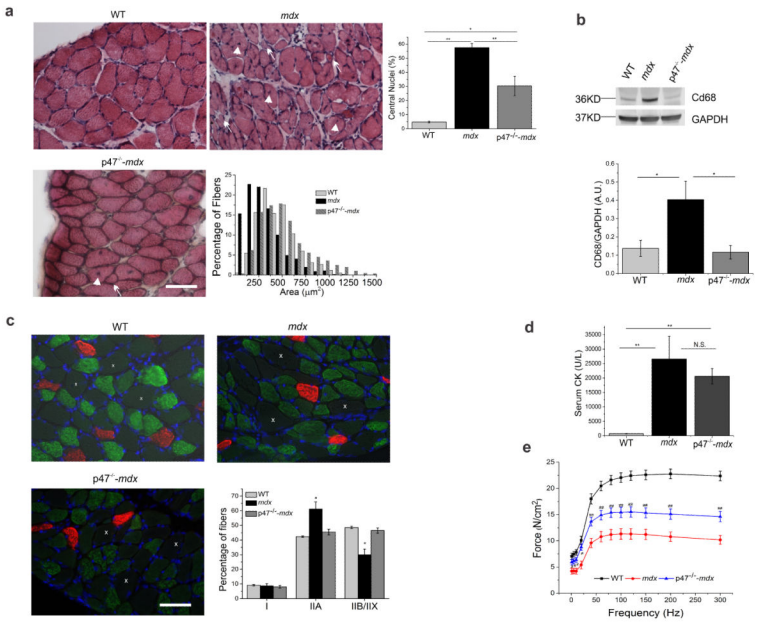

Figure 4. Genetic inhibition of Nox2-activity ameliorates pathological and functional phenotypes in dystrophic muscle

(a) Hematoxylin and eosin staining of cross-sections from diaphragm showing central nuclei (arrow head) and smaller fibers (arrow). **(b)** Immunoblot analysis of macrophage content (CD68). **(c)** Immunofluorecent and bright field images of diaphragm cross-sections showing fiber type distribution. Type I (red), IIA (green), IIB/IIX (white x, unstained and viewed from bright field overlay). (**d**) Serum creatine kinase activity. **(e)** Force frequency relationship in diaphragm muscle strips from WT (black), *mdx* (red), and p47$^{-/-}$-*mdx* (blue) mice. Scale bars represent 55 μm. For panel e, $^{\#}$ P<0.01 p47$^{-/-}$-*mdx* vs. *mdx*. $^{\#\#}$ P< 0.01 p47$^{-/-}$-*mdx* vs. WT and *mdx*. *Mdx* was statistically different than WT at all frequencies of stimulation. Statistical differences between groups were determined using ANOVA with Tukey's post-hoc test. *p < 0.05 and **p<0.01.

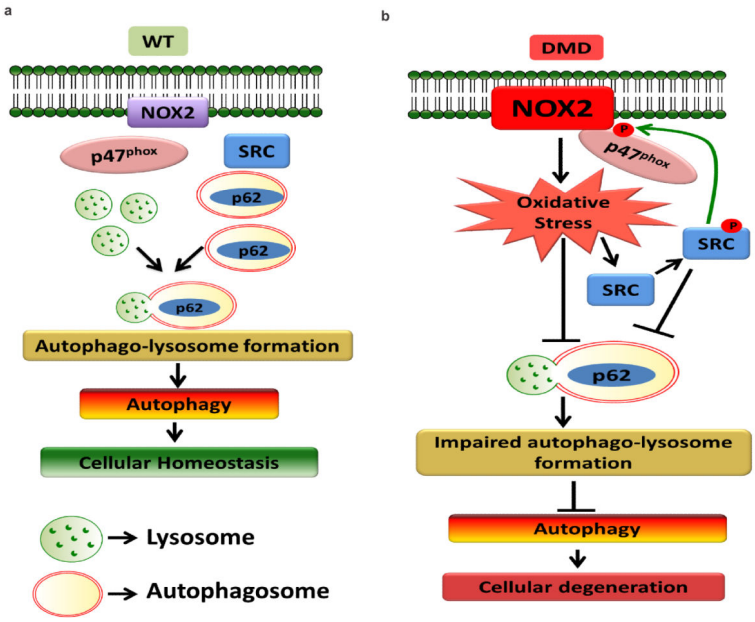

Figure 5. Proposed mechanism for Nox2/Src-dependent impaired autophagy in DMD pathology

(**a**) Autophagic machinery functions properly in WT condition through autophagosome and lysosome fusion, maintaining cellular homeostasis. (**b**) Upregulation of Nox2/Src-activity prevents autophago-lysosome formation, impairing autophagy and leading to cellular degeneration in DMD.